Calculation of monolayer structures of hydrocarbon chains on transition metal dichalcogenides: Dotriacontane on $MoSe_2$

S. Cincotti,* J. Burda,† R. Hentschke,‡ and J. P. Rabe§
Max-Planck-Institut für Polymerforschung, Postfach 3148, D-55021 Mainz, Germany
(Received 12 October 1994)

In situ scanning tunneling microscopy at the interface between atomically flat solid surfaces and solutions containing alkyl chains or alkyl derivatives show that the solute molecules often adsorb from solution to form dense crystalline monolayers at the liquid-solid interface. The structure of these layers depends on the nature of the substrate, and thus cannot be predicted from simple packing considerations alone. As an example of a theoretical approach to this problem on the atomic level, we present a calculation of the monolayer structure of dotriacontane on $MoSe_2$. We carry out energy minimizations of periodic clusters of dotriacontane on $MoSe_2$, where the potential energy is based on *ab initio* second-order Møller-Plesset perturbation calculations of the adsorbate-substrate interactions combined with a phenomenological force field description of the intra-adsorbate interactions. The resulting adsorbate structure is in excellent agreement with the experimentally observed structure.

PACS number(s): 68.45.−v, 61.16.Ch, 68.55.Jk

INTRODUCTION

In recent years considerable progress has been made refining the application of scanning probe microscopies to the study of highly ordered molecular films adsorbed on solid substrates (see, e.g., [1,2]). Such films, often simply self-assembled by adsorption from solution, are of interest in a variety of areas ranging from lubrication and colloidal stability over molecular recognition to tailoring the surface and interfacial properties of semiconductors [3]. Theoretical work on this subject currently lags behind in two key aspects, i.e., the *ab initio* prediction of the surface structure formed by a given type of molecule at a given interface as well as the relation between the observed tunneling or surface force contrasts and the atomic detail of the interfacial layer. In this work, we will be concerned with the first aspect. Using a combination of *ab initio* and phenomenological force field molecular mechanics calculations we study the monolayer structure of an *n* alkane, $C_{32}H_{66}$, physisorbed on the layered semiconductor surface of a transition-metal dichalcogenide, $MoSe_2$, for which experimental results have been obtained recently [4].

Computer modeling techniques like molecular dynamics and Monte Carlo are well suited to predict the translational and orientational ordering of rare gases and small molecules at smooth surfaces. Some examples, where, for instance, graphite is used as substrate, are Kr [5] or Ar [6], small linear molecules like N_2 [7] or CS_2 [8], polar molecules like CH_3F or CH_3Cl [9], and various hydrocarbons like methane [10], ethylene [11], ethane [12], benzene [13], butane [14], hexane [15], or decane [14]. For very dense overlayers composed of larger molecules, however, the straightforward simulation, starting with a random guess, which develops into the thermodynamically stable structure, is usually prohibitively time consuming. One should realize in this context that for monolayers formed via adsorption from solution, which is what we are interested in, the inclusion of the third dimension, i.e., the entire solid-solution interface, is necessary as a pathway for achieving the dense molecular arrangement on the surface [16,17], even though the coupling of the equilibrium monolayer structure to the adjacent solution may be weak [18,17]. In the present work we employ a molecular mechanics approach, which involves energetic comparisons within a physically plausible subset of the possible different monolayer structures of $C_{32}H_{66}$ on $MoSe_2$. In the following we proceed in two steps. First we derive a physisorption potential suitable for alkanes on $MoSe_2$ employing *ab initio* Møller-Plesset perturbation theory (MP2) cluster calculations. In a second part, we use this surface potential in conjunction with a phenomenological force field description of the intra-adsorbate interactions to calculate and to compare the potential energy of different plausible monolayer structures, including those based on previous scanning tunneling microscopy (STM) results for $C_{32}H_{66}$ physisorbed on graphite [19,20,18]. Our model proves capable of correctly reproducing the experimentally observed superstructure in STM images of $C_{32}H_{66}$ on $MoSe_2$ [4], and thus allows a theoretical understanding of the observed contrast patterns in terms of the underlying intra-adsorbate and adsorbate substrate interactions.

*Present address: Istituto di Elettrotecnica, Università di Cagliari, piazza D'Armi, 09123 Cagliari, Italy.
†Present address: Institute of Macromolecular Chemistry, Heyrovsky Sq. 2, 162 06 Prague 6, Czech Republic.
‡Corresponding author.
§Present address: Institut für Physikalische Chemie, Johannes-Gutenberg Universität, Jakob-Welder-Weg 11, D-55099 Mainz, Germany.

INTRA AND INTERMOLECULAR POTENTIAL DESCRIBING THE ADSORBATE-ADSORBATE AND ADSORBATE-SUBSTRATE INTERACTIONS

Here we adopt the same phenomenological force field approach, which we recently applied to the molecular dynamics simulation of ordered alkane chains physisorbed on graphite [18]. As in Ref. [18] we use the AMBER (assisted model building with energy refinement) [21,22] potential to describe the atomic interactions within the adsorbate, whereas the adsorbate-substrate interactions are calculated in terms of a Fourier summation over Lennard-Jones (LJ) atom-atom interactions extending over the solid [23]. Thus, the intra and intermolecular potential describing the adsorbate-adsorbate and adsorbate-substrate interactions is given by

$$V=\sum_{\text{bonds}} f_r(r-r_{\text{eq}})^2+\sum_{\text{angles}} f_\delta(\delta-\delta_{\text{eq}})^2 + \sum_{\text{dihedral}} f_n\{1+\cos(n\phi-\gamma)\} + \sum_{i<j}\sqrt{\varepsilon_i\varepsilon_j}\left\{\left[\frac{\sigma_i+\sigma_j}{r_{ij}}\right]^{12}-2\left[\frac{\sigma_i+\sigma_j}{r_{ij}}\right]^{6}\right\} + \sum_{i<j}\frac{q_iq_j}{r_{ij}}+\sum_i V_{\text{surf}}(\mathbf{r}_i)\,. \quad (1)$$

The first three terms are bonding intra-adsorbate interactions encompassing harmonic bond stretch and valence angle potentials as well as a cosine-type torsion potential. The next two nonbonded interaction terms describe electronic overlap and dispersion interactions via a simple 12-6 LJ potential and Coulomb interactions between atomic partial charges within the adsorbate. Notice that using the Lorentz-Berthelot mixing rules [24] the usual LJ parameters ε_{ij} and σ_{ij} are expressed as $\varepsilon_{ij}=\sqrt{\varepsilon_i\varepsilon_j}$ and $\sigma_{ij}=\sigma_i+\sigma_j$, where the indices label the interacting atoms and a factor $\frac{1}{2}$ on the right hand side of the expression for σ_{ij} has been absorbed into σ_i and σ_j. Notice also that following reference [21] the above 1-4 LJ and 1-4 Coulomb interactions, i.e., interactions between sites separated by three bonds, are scaled by a factor $\frac{1}{2}$. With the exception of the partial charges, which are adopted from previous work [18], all potential parameters entering into the intra-adsorbate interactions are adopted from the AMBER data base [21,22]. For the sake of completeness the parameters are compiled in Table I.

The last term in Eq. (1) describes the potential due to the surface acting on the adsorbate atoms located at $\mathbf{r}_i=(x_i,y_i,z_i)$. Notice that z_i is the perpendicular distance from the surface, defined with respect to the centers of mass of the atoms in the topmost layer plane. Steele [23] has shown for several surface geometries that for solids having a surface made up of a single type of exposed lattice plane $V_{\text{surf}}(\mathbf{r}_i)$ can be expressed in terms of a simple, rapidly converging Fourier series in terms of the lateral atomic positions with respect to the surface. Here we extend Steele's method to a family of transition metal dichalcogenides with a structure referenced as $2H_b$-MoS_2 [hexagonal $D_{6h}^4-P6_3/mmc$ (No. 194)] [25], which includes commonly used substrates like MoS_2, $MoTe_2$, WS_2, or WSe_2. Figure 1 shows a sketch of the corresponding (110) plane of this family of compounds as well as the layer structure normal to the (110) plane. In the following we assume that the interaction between the adsorbate and the substrate can be approximated in terms of pairwise LJ interactions, i.e., by $\varepsilon\{(\sigma/r)^{12}-2(\sigma/r)^6\}$, where ε is the potential well depth and σ is the location of its minimum. Utilizing the translational symmetry of

TABLE I. Potential parameters with the exception of the adsorbate-$MoSe_2$ potential parameters.

	Intra adsorbate parameters		
Bonds	f_r (kcal mol^{-1} Å^{-2})	r_{eq} (Å)	
C—C	310	1.53	
C—H	331	1.09	
Angles	f_δ (kcal mol^{-1})	δ_{eq}	
C—C—C	40	109.5°	
C—C—H	35	109.5°	
H—C—H	35	109.5°	
Dihedrals	f_n (kcal mol^{-1})	γ	n
x—C—C—x	1.3	0	3
LJ parameters	ε_i (kcal mol^{-1})	σ_i/Å	
C	0.12	1.85	
H	0.01	1.54	

Partial charges

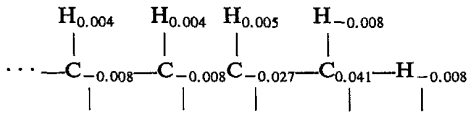

$MoSe_2$ parameters		
a=3.291 Å	c=12.91 Å	$d=c/8$

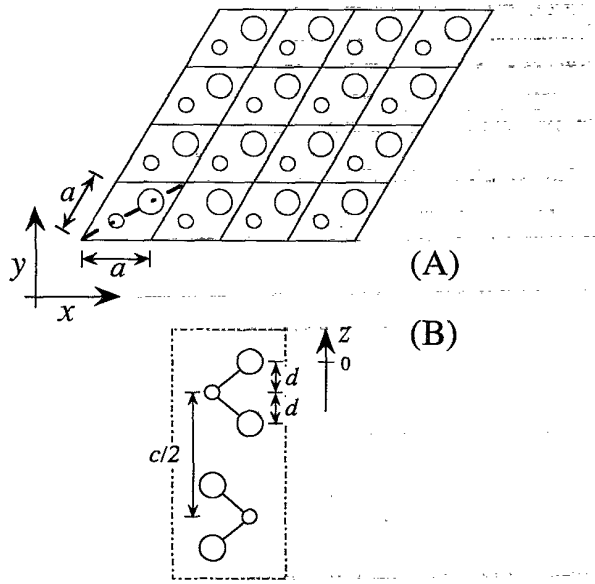

FIG. 1. $2H_b$-MoS_2 transition metal dichalcogenide. (A) Section of the basal plane containing 4×4 unit cells. Small circles indicate cations (here: Mo) and large circles indicate anions (here: Se). (B) Cut perpendicular to the basal plane along the long-short dashed line in the lower left unit cell in panel (A). The long-short dashed frame contains the repeat unit.

the substrate a calculation completely analogous to the one in Ref. [23] yields

$$V_{\rm surf}(\mathbf{r}_i)=V_0(z_i)+\sum_{m=1}^{\infty}V_m(\mathbf{r}_i)\ . \tag{2}$$

The right hand side of Eq. (2) is a sum of contributions from successively larger reciprocal neighbor shells corresponding to the two-dimensional surface lattice of interest. The first term, for instance, corresponds to $|\mathbf{g}|=g_0=0$, where $\mathbf{g}$ is a reciprocal surface lattice vector. This term is given by

$$V_0(z_i)=\frac{\pi}{a_s}\sum_{n=0}^{\infty}\left\{\varepsilon_{\rm chal}U_0\left[z_i+\frac{n}{2}c,\sigma_{\rm chal}\right]+\varepsilon_{\rm met}U_0\left[z_i+\frac{n}{2}c+d,\sigma_{\rm met}\right]+\varepsilon_{\rm chal}U_0\left[z_i+\frac{n}{2}c+2d,\sigma_{\rm chal}\right]\right\}, \tag{3}$$

where

$$U_0(z,\sigma)=\frac{\sigma^{12}}{5z^{10}}-\frac{\sigma^6}{z^4}\ . \tag{4}$$

Notice that Eq. (3) is the surface potential, which one obtains if, rather than summing over individual lattice sites in each surface plane, one simply integrates over homogeneously smeared out atom distributions within these planes and, subsequently, sums up these single plane contributions. Here each n, in fact, encompasses three surface planes. For instance, for $n=0$ the three terms in curly brackets in Eq. (3) are the contributions from the surface planes located at $z=0$, $-d$, and $-2d$ as shown in Fig. 1. In the present case chal and met stand for Se and Mo, respectively. The quantity $a_s=\sqrt{3}a^2/2$ is the area of the surface unit cell. Note that the lattice constant a as well as the two different layer spacings d and c are explained in Fig. 1. The additional terms in Eq. (2) for $m>0$ account for the surface corrugation, i.e., for the lateral variation of $V_{\rm surf}(\mathbf{r}_i)$. Analogous to Eq. (3) we have

$$V_m(\mathbf{r}_i)=\frac{\pi}{a_s}\sum_{n=0}^{\infty}\left\{f_m(x_i,y_i,\mu_{n,\rm chal})\varepsilon_{\rm chal}U_m\left[z_i+\frac{n}{2}c,g_m,\sigma_{\rm chal}\right]+f_m(x_i,y_i,\mu_{n,\rm met})\varepsilon_{\rm met}U_m\left[z_i+\frac{n}{2}c+d,g_m,\sigma_{\rm met}\right]+f_m(x_i,y_i,\mu_{n,\rm chal})\varepsilon_{\rm chal}U_m\left[z_i+\frac{n}{2}c+2d,g_m,\sigma_{\rm chal}\right]\right\}, \tag{5}$$

where now

$$U_m(z,g,\sigma)=\frac{\sigma^{12}}{1\,920}\left[\frac{g}{z}\right]^5K_5(gz)-\frac{\sigma^6}{2}\left[\frac{g}{z}\right]^2K_2(gz)\quad(m>0)\ , \tag{6}$$

and the K_v are modified Bessel functions. The terms containing the lateral spatial dependence are

$$f_m(x,y,\mu_{n,\xi})=2\sum_{(i_m,j_m)}\cos\left\{\frac{2\pi}{a}\left[i_m\left[x-\frac{y}{\sqrt{3}}-\mu_{n,\xi}\frac{a}{3}\right]+j_m\left[2\frac{y}{\sqrt{3}}-\mu_{n,\xi}\frac{a}{3}\right]\right]\right\}, \tag{7}$$

where ξ=met,chal, and $\mu_{n,\rm met}=1$, $\mu_{n,\rm chal}=2$ for $n=0,2,4,\ldots$, and $\mu_{n,\rm met}=2$, $\mu_{n,\rm chal}=1$ for $n=1,3,5,\ldots$. Note that the summation in Eq. (7) is over pairs of indices labeling reciprocal lattice sites on the mth neighbor shell, i.e.,

$$(i_m,j_m)=\begin{cases}(0,1)\ (1,1)\ (1,0) & \text{for } m=1\\ (2,1)\ (-1,1)\ (1,2) & \text{for } m=2\\ (2,0)\ (2,2)\ (0,2) & \text{for } m=3\\ \vdots\quad\vdots & \end{cases} \tag{8}$$

[cf. the corresponding expressions reported previously (for $m=1,5$) [23] for the (111) face of the fcc lattice]. Notice also that the magnitude of the reciprocal lattice vectors on the mth shell are given by

$$g_m=\frac{4\pi}{\sqrt{3}a}\sqrt{i_m^2+j_m^2-i_m j_m}\ . \tag{9}$$

It is important to note that the adsorbate-substrate LJ parameters in the Eqs. (3) and (5) depend on the type of the adsorbate atom at the position $\mathbf{r}_i$ even though, for simplicity, we do not indicate this by a separate index. As mentioned above, the surface potential [(2)–(9)] applies to a whole family of transition metal dichalcogenides. Here, however, we are solely interested in the physisorption of hydrocarbons on $MoSe_2$. For this case, the calculation of the adsorbate-substrate LJ parameters is discussed in the next section.

CALCULATION OF THE ADSORBATE-SUBSTRATE FORCE FIELD PARAMETERS

While the force field parameters for the intra-adsorbate interactions are taken from the AMBER data base [21,22], no reliable force field parameters are available for the adsorbate-substrate interaction. Thus here we use quantum chemical cluster calculations to obtain the numerical values for ε_ξ and σ_ξ (ξ=met, chal) in the above equations (3) and (5) describing the surface potential.

The cluster calculations are performed on the *ab initio* level using several small clusters consisting of a single $MoSe_2$ plus different small species (smsp), i.e., H_2, CH_4, and C_2H_6. The geometry of the $MoSe_2$ corresponds to the experimental solid state structure [25] as shown in Fig. 1, whereas for the (smsp), the optimized geometries are used. For each (smsp)-$MoSe_2$ cluster we calculate the energy $\Delta E(z)=E(z)-E(\infty)$, where here z is the normal separation between the first Mo plane and the center of mass of the respective (smsp) as indicated by the dashed lines in the insets in Fig. 2. $E(z)$ is the total cluster energy at the separation z, and $E(\infty)=[\text{smsp}]+E[MoSe_2]$ is the sum of the total energy of the optimized isolated (smsp) and the total energy of the isolated $MoSe_2$, for which we find that the triplet state should be taken as the ground state. Both energies were treated with BSSE (basis set superposition error) corrections. Notice that we calculate $\Delta E(z)$ for different z, keeping the orientation of the (smsp) fixed with respect to the $MoSe_2$ (as indicated in the insets in Fig. 2).

The total cluster energies $E(z)$ are calculated using the unrestricted Hartree-Fock method, including the second-order Møller-Plesset perturbation theory [26], keeping the molecular orbitals of the core electrons frozen. The MO-LCAO wave functions, which we use here, are based on the pseudopotentials developed by Hay and Wadt in connection with the double ζ basis set for the heavy atom valence electrons [27–29] and the Dunning-Huzinaga valence double ζ basis set [30] for carbon and hydrogen. For the numerical calculations we use the program HONDO 8 [31] implemented on DEC 3000/400AXP and IRIS Indigo workstations, respectively. The results of the *ab initio* calculations are summarized in Fig. 2, which shows $\Delta E(z)$ for the three different (smsp)-$MoSe_2$ clusters considered here.

In order to extract the adsorbate-substrate LJ parameters we fit $\Delta E(z)$ by a phenomenological cluster potential $V_{\text{cluster}}(z)$ of the form

$$V_{\text{cluster}}(z)=\sum_{\mu,\nu}\varepsilon_{\mu\nu}\left\{\left[\frac{\sigma_{\mu\nu}}{r_{\mu\nu}(z)}\right]^{12}-2\left[\frac{\sigma_{\mu\nu}}{r_{\mu\nu}(z)}\right]^{6}\right\}+\sum_{\mu,\nu}\frac{q_\mu q_\nu}{r_{\mu\nu}(z)}\ . \tag{10}$$

where μ and ν label (smsp)— and $MoSe_2$—atoms, respectively. Based on the values for $\Delta E(z)$ computed for different separations $z=z_i$, $i=1,\ldots,N_n$, shown in Fig.

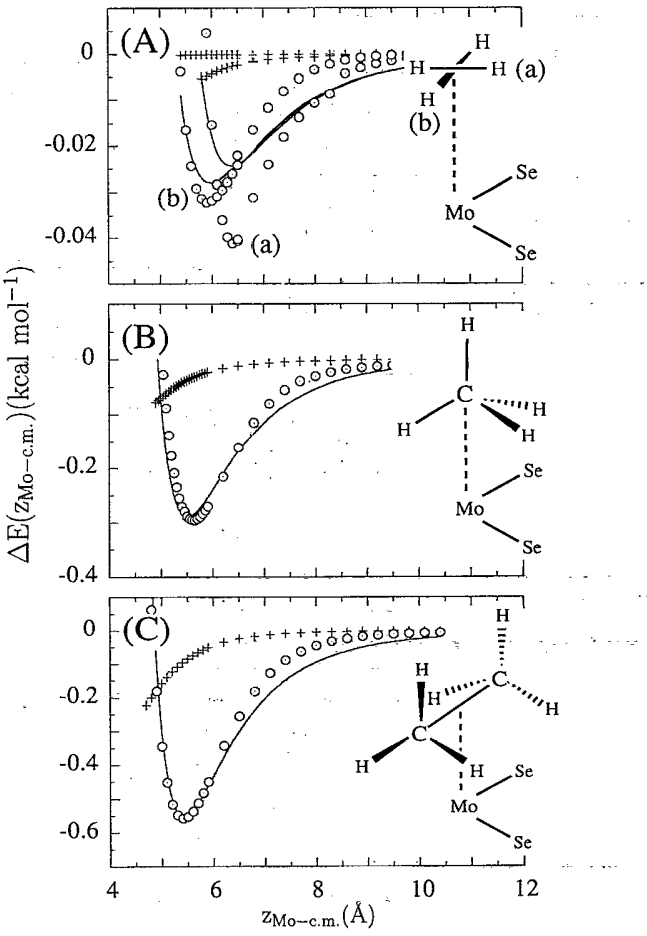

FIG. 2. Subtracted cluster energy $\Delta E(z)$ vs z. Here $z=z_{(\text{Mo-c.m.})}$ corresponds to the separation between the Mo atom and the respective centers of mass of H_2 (panel A), CH_4 (panel B), and C_2H_6 (panel C). The relative cluster geometries are shown in the inserts. Notice that the hydrogen results shown in panel (A) include two different orientations of the H_2 molecule (*a*) and (*b*). Circles indicate the quantum chemical *ab initio* results. The solid lines represent the Lennard-Jones contribution to the fits obtained using Eqs. (10) and (11), and the plusses are the Coulomb contributions using the *ab initio* partial charges as explained in the text.

TABLE II. Adsorbate-$MoSe_2$ LJ parameters as obtained by fitting Eq. (10) to the *ab initio* cluster results.

Adsorbate-$MoSe_2$ LJ parameters	H-Se	C-Se	H-Mo	C-Mo
$\varepsilon_{\mu\nu}$ (kcal mol^{-1})	7.18×10^{-4}	1.83	1.25×10^{-2}	7.45
$\sigma_{\mu\nu}$ (Å)	5.26	2.67	6.1	2.83

2, we carry out a steepest descent minimization of

$$\sum_{\text{smsp}} w(\text{smsp}) \sum_{i=1}^{N_n} \{V_{\text{cluster}}(z_i)-\Delta E(z_i)\}^2 , \qquad (11)$$

with respect to the LJ parameters $\varepsilon_{\mu\nu}$ and $\sigma_{\mu\nu}$. The weight factors w(smsp) are chosen roughly in proportion to the depths of the potential wells of the different (smsp)/$MoSe_2$ clusters. Notice that the summations in (11) extend over all 115 quantum chemical points calculated for the three different systems. The atomic partial charges q_μ and q_ν we compute via a Mulliken population analysis [32] of the self-consistent-field results (SCF) wave functions for each separation. The resulting values for $\varepsilon_{\mu\nu}$ and $\sigma_{\mu\nu}$ are compiled in Table II. In addition, the three panels of Fig. 2 show the respective fits of Eq. (10) to the quantum chemical results using the parameter values in Table II. Notice that the overall best fit is obtained for the C_2H_6-$MoSe_2$ cluster, which most closely corresponds to the systems of interest here. It should be emphasized that the parameters in Table II are not so much appropriate for each single atom-atom interaction separately, but rather for the overall adsorbate-substrate interaction. Notice also that even though the adsorbate-substrate Coulomb interaction is included in the fitting procedure, we neglect its contribution in Eq. (2), because the Coulomb contribution appears to be small for the relevant adsorbate-substrate separations. It is also worth noting that we have performed an additional calculation for one larger cluster, CH_4-$(MoSe_2)_4$, which did not indicate a significant dependence (in comparison to the overall error of the fitting procedure) of the LJ parameters on the substrate cluster size.

MODELING OF THE MONOLAYER STRUCTURE OF $C_{32}H_{66}$ ON $MoSe_2$

In this section we want to employ the above potential to model the equilibrium monolayer structure formed by $C_{32}H_{66}$ adsorbed on the basal plane of $MoSe_2$. In the experiment, dotriacontane, $C_{32}H_{66}$, is adsorbed from an organic solvent, 1-phenyloctane, onto $MoSe_2$, where the STM reveals a highly oriented monolayer [4]. As we have already mentioned, currently it is still prohibitively time consuming to carry out a dynamic molecular simulation, which includes the adsorption of $C_{32}H_{66}$ from solution together with the attendant ordering of the molecules into the experimentally observed monolayer structure [33,16]. Thus, here we take a simpler approach by comparing the potential energy of different $C_{32}H_{66}$ monolayers (with given plausible symmetries) physisorbed on the basal plane of $MoSe_2$ in the absence of solution. These molecular mechanics calculations are carried out based on the full potential described by Eqs. (1)–(9) using the parameters compiled in the Tables I and II.

Before we proceed with the full energy minimizations it is worth it to briefly discuss the surface potential $\sum_i V_{\text{surf}}(\mathbf{r}_i)$ for the simple case of a single isolated adsorbed methane molecule. Because we want to focus on the relative contributions coming from the different surface panes and reciprocal layer shells within these planes, we actually consider not the full methane molecule with its complicated orientation dependent adsorption energy, but rather a simplified "united atom" pseudomethane molecule, where the hydrogens are condensed into a single effective carbon atom C*. Thus $\sum_i V_{\text{surf}}(\mathbf{r}_i)$ is calculated for C* as for the full methane, but assuming that all methane atoms are located at $\mathbf{r}=\mathbf{r}_i$ ($i=1,\ldots,5$). In the following discussion of the adsorption energy of C* we implicitly assume this summation and write $V_{\text{surf}}(\mathbf{r})$ rather than $\sum_i V_{\text{surf}}(\mathbf{r}_i)$. $V_{\text{surf}}(\mathbf{r})$ as given by Eqs. (2)–(9) consists of a real space summation over equivalent layer planes parallel to the surface plus a summation over reciprocal neighbor shells within each of those layer planes. Figure 3(A) shows the leading term $V_0(z)$ of the C*/$MoSe_2$ interaction if only the first Se plane, the first Se plane plus the first Mo plane, the entire first $MoSe_2$ layer, the first two $MoSe_2$ layers, and finally all layers are included. Evidently, the first two lattice planes consisting of Se and Mo atoms, respectively, dominate the C*/$MoSe_2$ interaction, and the convergence of the summation over lower lying lattice planes is quite rapid. In particular, it is the first Mo plane, which contributes almost $\frac{2}{3}$ of the overall adsorption energy. Now we consider the corrugation terms $V_m(\mathbf{r})$—again for C*, but with a constant surface separation corresponding to the position of the minimum of $V_0(z)$ calculated including all layers. Figure 3(B) shows $V_m(\mathbf{r})$ including only the first Se plane and the first two reciprocal lattice shells, i.e., $m=1,2$. Notice that the contribution for $m=1$ strongly dominates. Figure 3(C) shows the contributions due to the $m=1$ terms of the first Mo plane and the second Se plane, respectively. This shows that the surface corrugation already is reasonably well described by taking into account the first Se plane with $m=1$ only. However, in the following we include the entire first $MoSe_2$ layer with $m=1$. Notice also that the overall amplitude of the corrugation is only about 15% of the potential well depth. It is also worth mentioning that the surface potential described by Eqs. (2)–(9) is not suited for calculations that require its frequent evaluation, even with the above approximation. For practical purposes it is useful to calculate and store $V_{\text{surf}}(\mathbf{r}_i)$ on a grid within a column, whose base is the surface unit cell and whose height is determined by the range of the surface potential normal to the surface (usually $\sim$15–20 Å are sufficient). From the stored values, $V_{\text{surf}}(\mathbf{r}_i)$ can be calculated quite rapidly

and accurately for any $\mathbf{r}_i$ by mapping $\mathbf{r}_i$ into the unit cell and a subsequent simple interpolation between the neighboring grid values of $V_{\text{surf}}(\mathbf{r}_i)$.

Now we consider one adsorbed $C_{32}H_{66}$ molecule. Figure 4 shows the variation of the surface potential $\sum_i V_{\text{surf}}(\mathbf{r}_i)$ along the x, y, and z direction for a single isolated all-trans $C_{32}H_{66}$ molecule, with its carbon zigzag plane parallel to the surface and its long axis oriented parallel to the x direction. Notice that the adsorption energy has a minimum at -80.1 kcal/mol, whereas the lateral variations of the surface potential are only about 0.3 kcal/mol along x and 6.5 kcal/mol along y. We can compare this to the case of n alkanes physisorbed on graphite, where an analogous calculation yields ~ 1.7 kcal/mol per CH_2 group (cf. Fig. 2 in Ref. [18]), whereas here we obtain ~ 2.5 kcal/mol per CH_2 group. Similarly, the corrugation is also more shallow on graphite, where the maximum amplitude is only about 40% of the corresponding maximum amplitude on $MoSe_2$.

For the full minimization we use Eqs. (1)–(9), i.e., we include all intra and intermolecular interactions in addition to the surface potential. We minimize the potential energy of a given structure employing a combination of the steepest descendent and the conjugated gradient method. Furthermore, all nonbonded interactions are omitted beyond a residue based cutoff of 10 Å, i.e., only the nonbonded interactions between residues that are wholly or partially contained within the cutoff sphere are included. Here each C_2H_4 group (or C_2H_5 group at the chain ends) constitutes a single residue. Note in this context that for the present system the effect of the weak Coulomb interactions is small compared to the short ranged van der Waals interactions.

We start by first considering 32 dotriacontane molecules, whose initial individual orientations with respect to the surface and molecular conformations coincide with

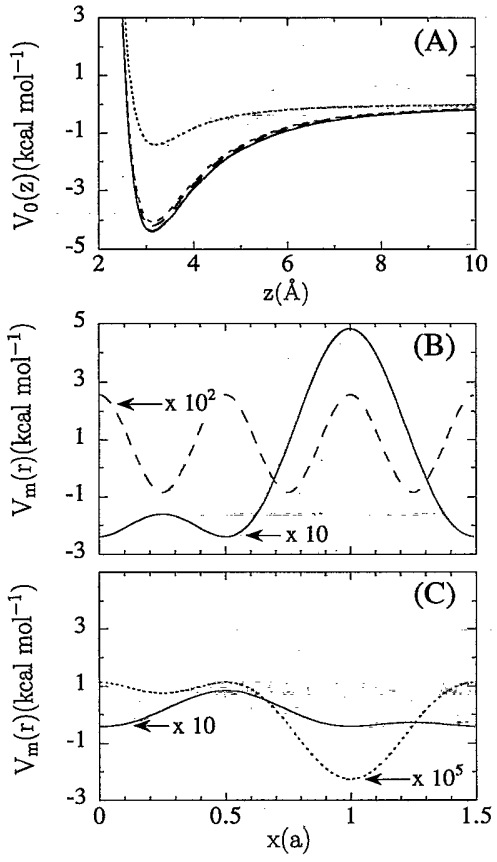

FIG. 3. Panel (A): $V_0(z)$ vs z for C*/$MoSe_2$ if only the first Se plane (dotted line), the first Se plane together with the first Mo plane (short dashed line), the first $MoSe_2$ layer (long dashed line), the first two $MoSe_2$ layers (dashed-dotted line), and finally all layers are included (solid line). Notice that the last two curves are virtually superimposed. Panel (B): $V_m(\mathbf{r})$ vs x for C*/$MoSe_2$ including only the first Se plane and the first two reciprocal lattice shells, i.e., $m=1$ (solid line), $m=2$ (dashed line). Notice that C* is moved along the long-short dashed line in the lower left unit cell in Fig. 1(A), where z is kept constant at the minimum of the solid potential curve of panel (A). Note that the two curves are scaled by the indicated factors. Panel (C): Curves corresponding to panel (B) for the case when the first Mo plane is considered with $m=1$ (solid line) or the second Se plane also with $m=1$ (dotted line). Notice again the scaling factors.

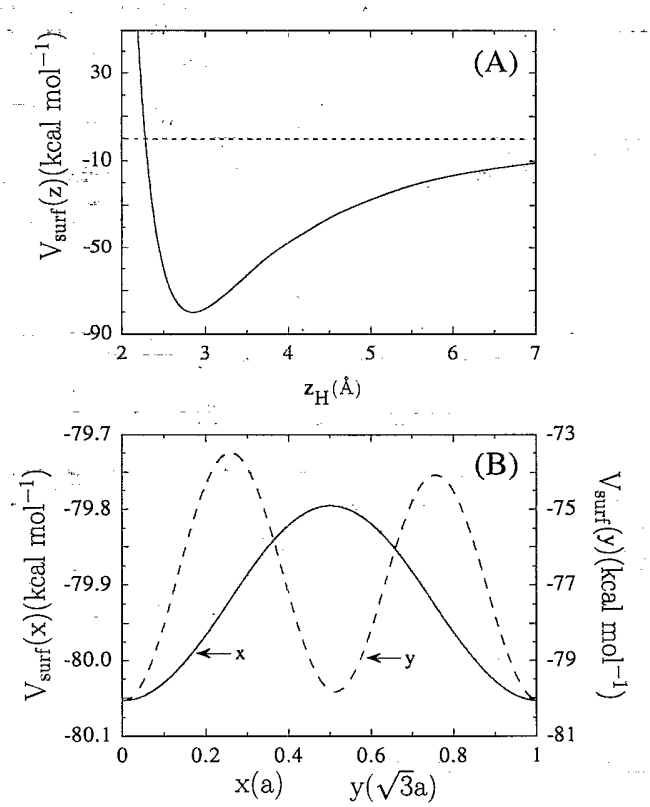

FIG. 4. Variation of the $MoSe_2$ surface potential along the x, y, and z directions for a single isolated all-trans $C_{32}H_{66}$ molecule, with its carbon zigzag plane parallel to the surface and its long axis oriented parallel to the x direction. Panel (A): Variation normal to the surface, where z_H is the separation between the substrate and the $C_{32}H_{66}$ hydrogens closest to the surface. Panel (B): Variation along the x (left axis) and y direction (right axis). Note that x and y here refer to translations along these directions for a single molecule whose z_H is fixed at the position of the potential minimum in panel (A).

the orientation and conformation of the isolated molecule discussed above, in a single lamellar arrangement. A sketch of this system is shown in Fig. 5(A). The close packed lamellar arrangement is the most plausible due to the pronounced shape anisotropy of the molecules, and it was also previously found for $C_{32}H_{66}$ physisorbed on graphite [19,20]. In addition, the perpendicular intermolecular separation Δ is taken to be 4.7 Å based on previous STM results [4], and all the molecules of dotriacontane lie with their carbon skeletons parallel to the substrate and are oriented along the x directions, which also corresponds to the minimum energy configuration of the above single $C_{32}H_{66}$. Figure 5(B) shows the minimized potential energy, applying free boundary conditions, as function of the angle γ between the long axis of the molecules and the direction defined by the lamella. The three minima around 90°, 60°, and 45° are to be expected, since neighboring zigzag chains lock in for a translation by 0, 2, and 4 methylene units, respectively [34]. The absolute minimum of the potential energy occurs at $\gamma=90°$, while the STM images [4] show that γ should be close to 60°. This result may be attributed to the fact that the observed tilt angle γ is significantly affected by the attractive intermolecular interaction between the adsorbed molecules, because, for free boundary conditions, decreasing γ reduces the contact area between neighboring molecules.

In order to provide the necessary intermolecular contact we consider a system in which 32 molecules now

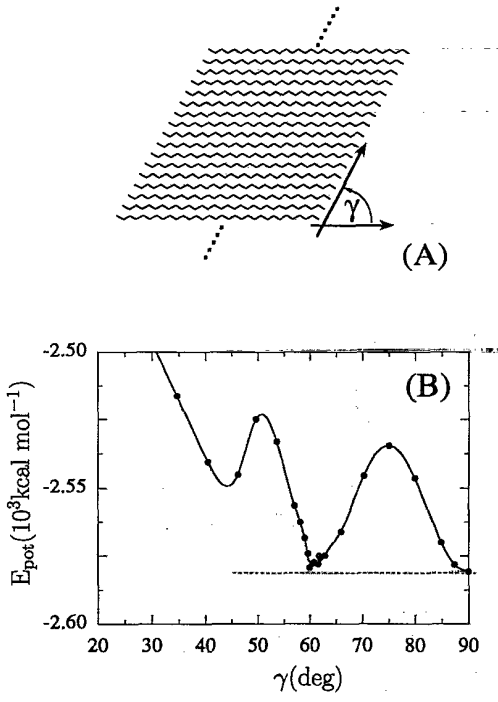

FIG. 5. Panel (A): Partial schematic of a single lamella with free boundaries consisting of 32 $C_{32}H_{66}$ molecules. Panel (B): The potential energy as function of the angle γ between the long axis of the molecules and direction defined by the lamella. The solid line is a spline fit through the calculated points indicated by the solid circles.

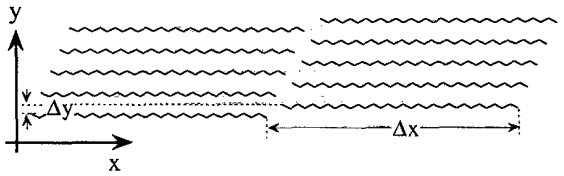

FIG. 6. Partial schematic of the system composed of four lamellae, each of which consists of eight molecules of $C_{32}H_{66}$. Notice that Δx and Δy, together with Δ (the separation along y between neighboring molecules within the same lamella), define the lamellar superstructure.

form four lamellae, each of which consists of eight molecules of dotriacontane as shown in Fig. 6. In addition, we employ periodic boundary conditions along the x direction, whereas the boundaries in y direction are still free. By doing this we avoid that the length of the free boundaries varies with γ. At this point it is also useful to introduce two additional parameters to fully characterize the monolayer unit cell, i.e., the lamellar repeat distance Δx and the offset between neighboring lamellae Δy (cf. Fig. 6). In the following we want to model these parameters based on the above potential. Figure 7(A) shows the plot of the potential energy for the system in Fig. 6 with

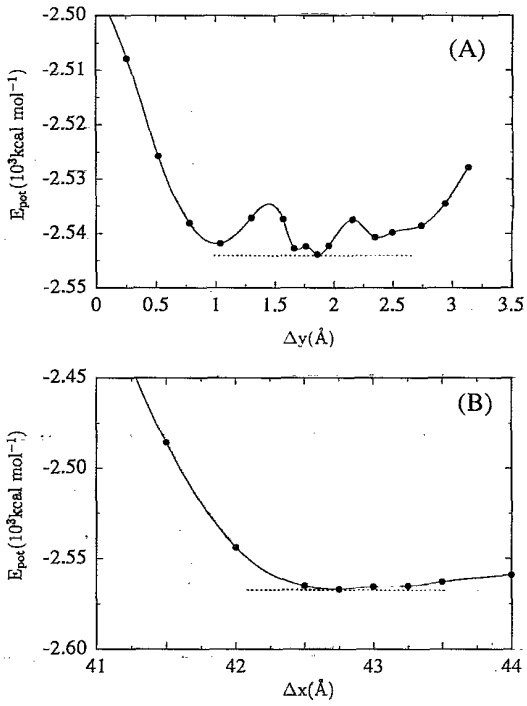

FIG. 7. The potential energy for the case of four lamellae consisting of eight molecules of $C_{32}H_{66}$ each as a function of the parameters Δx and Δy in Fig. 6. Panel (A): The potential energy as a function of Δy for $\gamma=60°$ and $\Delta x=42.0$ Å. Panel (B): The potential energy as a function of Δx for $\gamma=60°$ and $\Delta y=1.765$ Å. In both cases, periodic boundary conditions are applied in the x direction only (cf. Fig. 6). Again, the solid lines are spline fits through the calculated points indicated by the solid circles.

periodic boundary conditions along x as a function of the interlamellar offset Δy along the y direction. Here we have fixed the angle γ at 60° (corresponding to the STM results). The lamellar width Δx is also kept constant at 42 Å, which slightly exceeds the length of an all-trans $C_{32}H_{66}$ molecule, and, in addition, $\Delta = 4.7$ Å as in the above case for the single free lamella. In this plot the potential energy exhibits a minimum at $\Delta y = 1.765$ Å. Using again $\gamma = 60°$ but now $\Delta y = 1.765$ Å, Fig. 7(B) shows the potential energy as a function of Δx. In this case, the minimum occurs at $\Delta x \sim 42.75$ Å. These values for Δx and Δy are in good agreement with the STM results. In particular, experimentally (cf. the STM image in Fig. 8) one finds a y offset between neighboring lamellae, which is close to $\frac{1}{3}$ of the intermolecular separation Δ, i.e., $\Delta/3 = 1.6$ Å, which is in good accord with the above value for Δy.

Finally, we return to vary the tilt angle γ to check the consistency of the above results. Again we use the system sketched in Fig. 6, with periodic boundary conditions along the x direction only. The result for $\Delta x = 42.75$ and $\Delta y = 1.765$ Å is shown in Fig. 9. In contrast to the case of the single lamella with free boundaries, we now obtain the deepest minimum in the potential energy for $\gamma = 62°$, which is in excellent agreement with the experimentally observed lamellar tilt [4].

So far we have only dealt with the xy structure of the absorbed monolayer. However, the STM image in Fig. 8 also shows a contrast modulation along the lamellae with a periodicity extending over a little less than three molecules. The present study shows that this contrast modulation may be understood in terms of a modulation of the adsorbate-substrate separation. Figure 10 shows a plot of the z positions of the $C_{32}H_{66}$ carbon skeletons along the lamella corresponding to the minimum potential energy configuration in Fig. 9, where we have averaged over the four lamellae considered here. The figure shows a clearly discernible periodicity of about three molecules, in good accord with the experimental observation. Moreover, as previously introduced [4], this periodicity in the STM images is the basis for the assumed intramolecular distance.

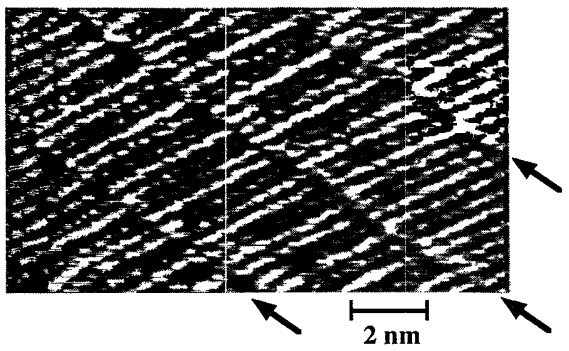

FIG. 8. STM image of a $C_{32}H_{66}$ monolayer on $MoSe_2$ (cf. Fig. 2(b) in Ref. [4]). The arrows indicate the lamella boundaries. Notice that the angle between the lamellae and the long axis of the molecules is $\gamma \approx 60°$, and that the offset between neighboring lamellae is about $\frac{1}{3}$ of the intermolecular separation.

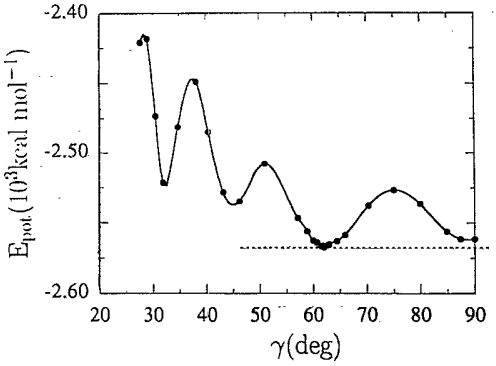

FIG. 9. The potential energy of the structure sketched in Fig. 6 as a function of the tilt angle γ between the lamellar axis and the long axis of the molecules within the lamella for $\Delta x = 42.75$ Å and $\Delta y = 1.765$ Å applying periodic boundaries along the x direction only. As in Fig. 5 the solid line is a spline fit through the calculated points indicated by the solid circles.

CONCLUSION

In conclusion, our model based on a phenomenological intra-adsorbate force field in combination with an adsorbate-substrate interaction derived from *ab initio* cluster calculations is capable of explaining the packing

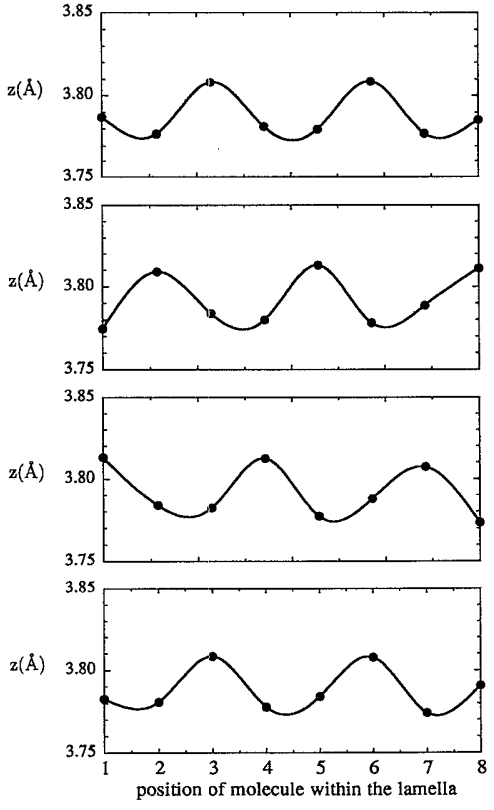

FIG. 10. Average z position of the $C_{32}H_{66}$ carbons along the lamellae corresponding to the minimum in the potential energy shown in Fig. 9. The lamella are numbered from left to right, while the molecules within each lamella are numbered from bottom to top (see Fig. 6). As before, the solid lines are spline fits through the calculated points indicated by the solid circles.

of a long chain alkane on the basal plane of $MoSe_2$, which in comparison to graphite is distinguished by a much larger adsorption energy and surface corrugation. Moreover, it explains a superstructure present in the STM images of alkanes on $MoSe_2$. The two main approximations that we have made are the neglect of entropic contributions to the free energy as well as the replacement of the solid-monolayer-solution interface by the solid-monolayer-vacuum interface. With respect to the former, we have shown in a previous simulation of $C_{24}H_{50}$ on graphite [18] that the orientation of the carbon zigzag plane with respect to the surface may indeed be entropically driven even within a dense crystalline packing. Therefore here we have taken the orientation of the zigzag plane as concluded from experimental evidence [4]. With respect to the second approximation, we have also previously shown for heptane-benzene mixtures in contact with graphite [17] that the coupling of the structure and dynamics of the layer in direct contact with the surface with the rest of the solution is quite weak. This is not too surprising because the interaction of graphite with the immediate surface alkane layer is significantly stronger than the alkane-alkane interaction [18]. Finally, we like to emphasize that the method used here and, in particular, the equations for the surface potential can be straightforwardly applied to hydrocarbon monolayers on a number of other transition metal dichalcogenides (cf. above), like alkanes and alkyl derivatives observed on MoS_2 [35]. In this case the MoS_2 hydrocarbon interactions of course must be calculated separately, where, however, again the same general approach may be used.

ACKNOWLEDGMENT

This work has been supported in part by ESPRIT Basic Research Project 7282 (TOPFIT).

[1] H. J. Butt, R. Guckenberger, and J. P. Rabe, Ultramicroscopy **46**, 375 (1992).
[2] J. P. Rabe, S. Buchholz, and L. Askadskaya, Phys. Scr. **T49**, 260 (1993).
[3] J. D. Swalen, D. L. Allara, J. D. Andrade, E. A. Chandros, S. Garoff, J. Israelachvili, T. J. McCarthy, R. Murray, R. F. Pease, J. F. Rabolt, K. J. Wynne, and H. Yu, Langmuir **3**, 932 (1987).
[4] S. Cincotti and J. P. Rabe, Appl. Phys. Lett. **62**, 3531 (1993).
[5] F. F. Abraham, W. E. Rudge, D. J. Auerbach, and S. W. Kock, Phys. Rev. Lett. **52**, 445 (1984).
[6] L. A. Rowley, D. Nicholson, and N. G. Parsonage, Mol. Phys. **31**, 365 (1976).
[7] W. A. Steele, A. V. Vernov, and D. J. Tildesley, Carbon **25**, 7 (1987).
[8] Y. P. Joshi, D. J. Tildesley, J. S. Ayres, R. K. Thomas, Mol. Phys. **65**, 991 (1988).
[9] C. J. Ruiz-Suarez, M. L. Klein, M. A. Moller, P. A. Rowtree, G. Scoles, and J. Xu, Phys. Rev. Lett. **61**, 710 (1988).
[10] E. S. Severin and D. J. Tildesley, Mol. Phys. **41**, 1401 (1980).
[11] S. Nosè and M. L. Klein, Phys. Rev. Lett. **53**, 818 (1984).
[12] M. A. Moller and M. L. Klein, J. Chem. Phys. **90**, 1960 (1989).
[13] R. Hentschke and B. L. Schürmann, Surf. Sci. **262**, 180 (1992).
[14] S. Leggetter and D.J. Tildesley, Mol. Phys. **68**, 519 (1989).
[15] F. Y. Hansen, J. C. Newton, and H. Taub, J. Chem. Phys. **98**, 4128 (1993).
[16] T. K. Xia and U. Landman, Science **261**, 1310 (1993).
[17] M. J. Kotelyanskii and R. Hentschke, Phys. Rev. E **49**, 910 (1994).
[18] R. Hentschke B. L. Schürmann, and J. P. Rabe, J. Chem. Phys. **96**, 6213 (1992).
[19] G. C. McGonigal, R. H. Bernhardt and D. J. Thomson, Appl. Phys. Lett. **57**, 28 (1990).
[20] J. P. Rabe and S. Buchholz, Science **253**, 424 (1991).
[21] S. J. Weiner, P. A. Kollman, D. A. Case, U. C. Singh, C. Ghio, G. Alagona, S. Profeta, and P. Weiner, J. Am. Chem. Soc. **106**, 765 (1984).
[22] S. Weiner, P. Kollman, D. T. Nguyen, and D. A. Case, J. Comput. Chem. **7**, 230 (1986).
[23] W. A. Steele, Surf. Sci. **36**, 317 (1973).
[24] J.-P. Hansen and I. R. McDonald, *Theory of Simple Liquids*, 2nd ed. (Academic, London, 1986).
[25] F. Hulliger, *Structural Chemistry of Layer-Type Phases* (Reidel, Dordrecht, Holland, 1976), Vol. 5.
[26] C. Møller and M. S. Plesset, Phys. Rev. **46**, 618 (1934).
[27] W. R. Wadt and P. J. Hay, J. Chem. Phys. **82**, 284 (1985).
[28] P. J. Hay and W. R. Wadt, J. Chem. Phys. **82**, 270 (1985).
[20] P. J. Hay and W. R. Wadt, J. Chem. Phys. **82**, 299 (1985).
[30] T. H. Dunning and P. J. Hay, *Modern Theoretical Chemistry* (Plenum, New York, 1976), p. 28.
[31] M. Dupuis, A. Fazazel, S. P. Karna, and S. A. Maluedes, in *Modern Techniques in Computational Chemistry*, edited by E. Clementi (ESCOM, Leiden, 1989), p. 277.
[32] R. S. Mulliken, J. Chem. Phys. **23**, 1833 (1955).
[33] R. Hentschke and R. Winkler, J. Chem. Phys. **99**, 5528 (1993).
[34] A. I. Kitaigorodsky, *Molecular Crystals and Molecules* (Academic, London, 1973).
[35] S. Cincotti and J. P. Rabe, *Supramolecular Science* (to be published).